

ACTNET: end-to-end learning of feature activations and aggregation for effective instance image retrieval

Syed Sameed Husain, Eng-Jon Ong and Miroslaw Bober, *Member, IEEE*

Abstract—We propose a novel CNN architecture called ACTNET for robust instance image retrieval from large-scale datasets. Our key innovation is a learnable activation layer designed to improve the signal-to-noise ratio (SNR) of deep convolutional feature maps. This works in tandem with multi-stream aggregation, where complementary deep features from different convolutional layers are transformed and balanced, using our novel activation layer, before aggregation into a global descriptor. Importantly, the learnable parameters of activation blocks are explicitly trained, jointly with the CNN parameters, in an end-to-end manner minimising triplet loss. This means that our network jointly learns the CNN filters and their optimal aggregation for the retrieval task. To our knowledge, this is the first time parametric functions are used to control and learn optimal aggregation. We conduct an in-depth experimental study on three non-linear activation functions: Sine-Hyperbolic, Exponential and modified Weibull, showing that while all bring significant gains the Weibull function performs best thanks to its ability to equalise strong activations. The results clearly demonstrate that activation functions significantly enhance the discriminative power of deep features, leading to state-of-the-art retrieval results.

Index Terms—Image retrieval, global image descriptor, Convolutional Neural Network, deep features, activation functions, compact image signature



1 INTRODUCTION

LAST decade has seen an explosive growth in the usage of multimedia. Early solutions to the management of these huge volumes of multimedia fell below expectations, stimulating active research in areas such as instance image retrieval (IIR). Instance image retrieval is crucial for many applications including mobile visual search, augmented reality, robotic vision, automotive navigation, mobile commerce, surveillance and security, content management and medical imaging, and it will only grow in importance as AI systems proliferate. In IIR, the aim is to retrieve images depicting instances of a user-specified object in a large unordered collection of images. The task is challenging as the objects to be retrieved are often surrounded by background clutter, or partially occluded. Additionally, variations in objects appearance exist due to illumination and view-point changes. Consequently, one requires robust techniques that can cope with significant variability of local image measurements. Furthermore, today's systems must be scalable due to the overwhelming volumes of multimedia data.

In order to overcome these challenges, a robust and compact mathematical representation of an image is necessary. While Convolutional Neural Networks (CNN) have become essential components in the best performing methods for many computer vision tasks including image classification, they have failed so far to achieve desirable results in image retrieval task, especially on large-scale datasets. We attribute the underwhelming retrieval performance of deep methods to three main reasons: (1) suboptimal aggregation framework to compute global image descriptor from dense convolutional features, (2) inappropriate training procedure of

deep network resulting in substandard learning of difficult cases, and (3) computationally expensive deep models that are not suitable for real world applications.

Our solution to solve above problems is to develop a deep neural network called Activation Network (ACTNET) which is trained in an end-to-end manner to improve retrieval accuracy. The main contributions of the article are:

- we propose a novel trainable activation layer that improves the signal-to-noise ratio (SNR) of deep convolutional feature map. We conduct an in-depth experimental study to illustrate the effects of applying three non-linear activation functions: Sine-Hyperbolic, Exponential and modified Weibull. The results show that activation function significantly enhance the discriminative power of convolutional features, leading to world class retrieval results.
- we design a multi-layer CNN architecture (ACTNET) where deep features from different convolutional layers are transformed using our novel activation layer and then aggregated into a single global descriptor. Importantly, the trainable parameters from multiple CNN layers including the parameters of activation blocks are explicitly trained in an end-to-end manner minimising the triplet loss.
- we develop a low-latency, small-memory and low-power ACTNET model for real world applications. Detailed experimental results show that our low-complexity ACTNET achieves comparable performance to the state-of-the-art RMAC [1] and GEM [2] CNNs while providing five times faster extraction speed.
- we perform extensive experiments on several

S. Husain, E.Ong and M. Bober are with University of Surrey, Guildford, Surrey, UK. E-mails: {sameed.husain, e.ong, m.bober}@surrey.ac.uk

datasets and show that ACTNET outperforms the best CNN-based methods: MAC [3], RMAC [1] and GEM [2].

The ACTNET model generates robust and compact global descriptor that works extremely well for instance image retrieval. At the base, it uses a CNN (ResNext [4] or MobileNet [5]) as a powerful convolutional feature extractor. These deep features are aggregated using novel activation layer, average pooling layer and PCA+Whitening layer, into a single image signature. The ACTNET is trained in an end-to-end manner using Stochastic Gradient Descent (SGD) with the triplet loss function to optimise retrieval performance. The proposed method achieves retrieval performances of 95.1%, 91.4%, 72.7%, 52.2%, 80.7% and 62.7% on Holidays, Oxford5k, *ROxfM*, *ROxfH*, *RParM* and *RParH* datasets, outperforming the latest state-of-the-art methods including those based on computationally costly local descriptor indexing and spatial verification.

The paper is organised as follows. Section 2 presents the literature review of existing methods. Section 3 presents in detail our novel ACTNET. The experimental setup and the extensive evaluation of ACTNET is presented in Section 4. In Section 5 we compare our results with the state-of-the-art demonstrating significant improvement over recent global descriptors on all retrieval datasets. Finally, Section 6 concludes the paper.

2 RELATED WORK ON IMAGE RETRIEVAL

This section presents an overview of systems that have contributed significantly to instance image retrieval.

2.1 Classical image retrieval

Classical techniques to IIR involve aggregating scale-invariant hand-crafted descriptors such as SIFT [6] or SURF [7] into a single global image descriptor for fast matching. The most popular global representations that encode the distributions of local descriptors in an image are Bag of Features (BoF) [8], Fisher Vectors (FV) [9], Vector of Locally Aggregated Descriptors (VLAD) [10], Triangulation Embedding (TEmb) [11] and Robust Visual Descriptor (RVD) [12]. In BoF, each image is represented as a histogram of visual word occurrences. Fisher Vector encodes descriptors based on Fisher-Kernel framework; VLAD is a simplified version of FV, computed by aggregating the residual vectors between the local descriptors and their corresponding visual words. The TEmb representation encodes descriptors using democratic aggregation while RVD uses rank-based multi-assignment and direction preserving mapping to aggregate descriptors. Several advancements have been made to improve the performance of global representations such as incorporating large visual vocabulary [13], [14], query expansion [15], [16] and spatial verification [13].

The methods based on hand-crafted descriptors fail to achieve the desired retrieval performance due to their lack of robustness to non-linear image transformations such as partial occlusions and significant view point and illumination changes.

2.2 Deep CNN image retrieval

Recent approaches to IIR use deep convolutional features of CNN, typically trained for ImageNet classification, to compute global image representations. Azizpour et al. [17] performs max-pooling while Babenko et al. [18] applies sum-pooling to the last convolutional features of VGG16 [19]. One step improvement is the cross-dimensional weighted sum-pooling of Kalantidis et al. [20]. Popular aggregation methods such as Fisher Vectors, VLAD and RVD are adapted to encode deep features in the work of Ong et al. [21], Arandjelovic et al. [22] and Husain et al. [12]. Toliás et al. [3] develop a hybrid scheme called Regional Maximum Activations of Convolutions (RMAC), where last convolutional layer features are first max-pooled over regions using fixed grid. The regional features are PCA+whitened, L2-normalised and sum aggregated to form image signature. A modified version of RMAC that combines multi-scale and multi-layer features extraction is introduced by Seddati et al. [23]. The method of Jimenez et al. [24] uses VGG16 and class activation maps to compute global descriptor. Xu et al. [25] propose semantic-based aggregation approach where probabilistic proposals corresponding to special semantic content in an image are used to aggregate deep features. A hybrid deep feature aggregation method that unifies sum and weighted pooling to compute an image representation is presented by Pang et al. [26].

The methods that use convolutional features from CNN, trained for ImageNet classification, perform sub-optimally for IIR due to CNN being tuned to optimise intra-class generalisation. Current methods aim to solve this problem by finetuning the networks for retrieval task.

2.3 Finetuned deep CNN image retrieval

Arandjelovic et al. [22] introduce NetVLAD where the last convolutional layer of VGG16 is followed by a generalised VLAD layer and the whole architecture is trained using weakly supervised triplet loss. Gordo et al. [1] build on the core RMAC network and train the deep image retrieval (DIR) architecture on Landmarks dataset with triplet loss. Radenovic et al. [2] propose to aggregate deep features using generalised mean pooling (GEM) layer. More precisely, the GEM layer is added to the last convolutional layer of ResNet101 and the resultant architecture is trained on Landmarks dataset to minimise contrastive loss. Two variants of GEM pooling are weighted generalised mean pooling (WGEM) [27] and attention-aware generalised mean pooling (AGEM) [28]. Xu et al [29] develop an adversarial soft-detection-based aggregation (ASDA) network which aggregates deep features using adversarial detector and soft region proposal layer. Teichmann et al. [30] propose to aggregate and match deep local features (DELf) based on regional aggregated selective match kernels (R-ASMK). In [31], Husain et al. propose state-of-the-art CNN called REMAP in which multi-layer regional features are aggregated based on entropy-guided pooling.

In summary, while a very significant progress has been achieved recently, the retrieval performance of the state-of-the-art methods is still underwhelming, especially on challenging large-scale datasets, where many distractor images resembling the query image, but depicting a different

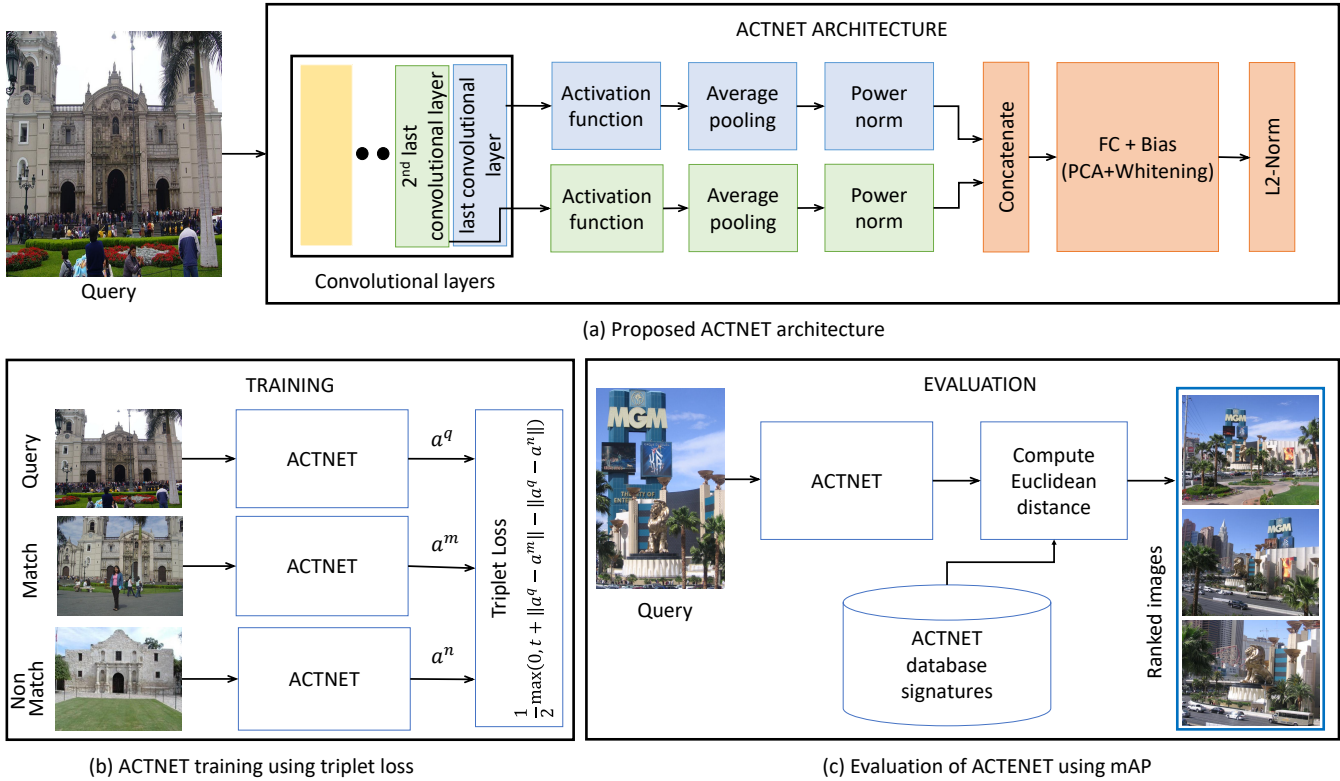


Fig. 1. (a) Proposed ACTNET architecture with multi-layer activation based aggregation, (b) training of ACTNET using triplet loss and (c) evaluation of ACTNET on state-of-the-art datasets

object, exist. We attribute this weakness to three main reasons, which our present work addresses, namely: (1) CNN architectures, and in particular the design of the aggregation stage which is responsible for robust global descriptor generation, (2) training protocols resulting in sub-optimal learning of the extreme cases, and (3) mapping of the deep representations onto compact signatures, which may lead to the reduction of its discriminatory power.

3 ACTIVATION NETWORK

In this section, we address the aforementioned issues by designing a deep and differentiable architecture ACTNET which is trained in an end-to-end manner to optimise retrieval task.

In our first contribution, we develop an activation based aggregation mechanism for deep descriptors, inspired by the concepts of core signal processing. The final convolutional layer of CNN acts as a powerful signal generator that extracts important features of an image, often contaminated with the background noise. The aim is to maximise the signal-to-noise ratio (SNR) of the convolutional feature map i.e to amplify the signals from the actual object in an image relative to the background noise. This is achieved by passing the responses of convolutional layer through a learnable non-linear activation function, before aggregation into a global descriptor. We perform an in-depth experimental study to analyse the effects of applying three differentiable activation functions: Sine-Hyperbolic, Exponential and modified Weibull. The results show that activation functions significantly enhance the robustness

and discriminative power of deep features, leading to the state-of-the art retrieval performance.

Our second contribution is to design a deep multi-layer architecture, called Activation Network (ACTNET), to optimise retrieval task. In ACTNET, multiple parametric activation layers operate in tandem with multi-stream aggregation, where a hierarchy of deep features from different convolutional layers are enhanced using activation functions and optimally aggregated into a discriminative global signature. The ACTNET architecture is trained in an end-to-end manner, where the convolutional weights, activation parameters and PCA+Whitening weights are trained with triplet loss. The key aspect is that the network learns the activations across multiple-layers during training to represent complementary and distinct levels of visual abstractions, improving retrieval performance.

While the image retrieval systems have shown remarkable speed and performance on GPU-based computers, our aim is to deliver an efficient and effective system into the hands of mobile users. In the third contribution, we develop a low power, low latency and small memory footprint ACTNET suitable for running on mobile devices. The low-complexity Mobile-ACTNET achieves comparable performance to computationally expensive methods GEM [2] and RMAC [1] while having five times faster descriptor extraction speed.

The ACTNET, presented in Figure 1a, consists of a baseline CNN (pre-trained on ImageNet) followed by our aggregation network. Any CNN can serve as the base however we show the results on two networks: the best performing

ResNext101 [4] and low-complexity MobileNetV2 [5]. For these CNNs, only the convolutional layers are retained, with the fully connected layers for classification discarded. The outputs of the final convolutional layers are each fed to separate “aggregation streams” that involve our proposed activation layer. Details of the multi-stream activation layer is presented in Section 3.1. In each stream, the activation function is followed by average pooling and power normalisation layer. The outputs of both streams are then recombined in a concatenation layer. This is followed by a PCA+Whitening layer before the final L2-normalisation layer for producing the global descriptor of an image. The training procedure (shown in Figure 1b) adopts a three stream siamese architecture where the image signatures extracted by each of the streams are jointly considered by the triplet loss function. The training procedure for the ACTNET is described in Section 3.4. In the evaluation phase (Figure 1c), an ACTNET signature is computed from a query image and compared against a database of pre-computed signatures. Based on the similarity score, the database images are ranked and mean Average Precision (mAP) is computed.

3.1 Learnable non-linear activation layer

In this section, we will describe a novel CNN layer which we call ‘activation layer’ that carries out operations analogous to a learnable activation function. Our activation layer provides the ability to learn and tune non-linear activation functions. The aim is to give greater emphasis to important responses from the object in an image and reduce the impact of background noise by non-linearly scaling the values of the input tensor. Crucially, this non-linear scaling should be tuneable during the learning process.

The fundamental difference in our work and state-of-the-art on developing adaptive activation functions is that we aim to improve the SNR of the final convolutional feature map before aggregation into a global descriptor while the latter focuses on improving the speed and stability of the network. Our activation function non-linearly increases convolutional layer values within a real-valued interval and the non-linear rate of increase is optimised during the training process to improve the retrieval task. Recent works on using activation functions to help fast training of CNN are [32], [33], [34], [35], [36]. The rectified linear activation (ReLU) function [33] has made it easier to effectively train a DNN compared to activation functions such as sigmoid or tanh, by addressing the problem of vanishing gradients. Agostinelli et al. [36] propose to use an adaptive linear piecewise model for the activation function. Recently, Farhadi et al. [36] propose an adaptive ReLU function that provides a smoother scaling increase of activation values. Qian et al. [35] explore methods to linearly and non-linearly combine basic activation functions.

We denote the non-linear activation function as $\phi(\mathbf{X}; \theta_\phi, \mathbf{w}_\theta)$, where $\phi : \mathbb{R}^{W \times H \times D} \rightarrow \mathbb{R}^{W \times H \times D}$ is an operation that takes as input a tensor \mathbf{X} of size $W \times H \times D$ and applies an associated real-valued function $\theta_\phi : \mathbb{R} \rightarrow \mathbb{R}$ to each element of the input tensor. Importantly, we consider parameterised functions for θ_ϕ , where its respective

parameters are denoted as a vector of real values: \mathbf{w}_θ . More specifically, we have:

$$\phi(\mathbf{X}; \theta_\phi, \mathbf{w}_\theta) = (\theta_\phi(x_{ijk}; \mathbf{w}_\theta))_{i,j,k=1}^{W,H,D}$$

In this work, we have considered three different activation functions for θ_ϕ : Sine-Hyperbolic, Exponential and modified Weibull. These three are chosen due to the following properties that they have in common:

- Each activation function non-linearly and monotonically increases input values within a real-valued interval. This allows us to place greater emphasis on larger values (important activations), compared to a linear scaling.
- The non-linear rate of increase is adjustable for learning purposes. As such, all the activation functions considered are parameterised.
- Finally, for use in a stochastic gradient descent framework, we require all chosen functions to be differentiable with respect to their parameters.

We next give the details of the three different activation functions used in ACTNET CNN. For clarity and convenience, we will omit writing the vector of parameters, \mathbf{w}_θ , when describing the activation function, writing it as $\theta_\phi(x)$ instead of $\theta_\phi(x; \mathbf{w}_\theta)$.

Sine-Hyperbolic function (SinH)

The first activation function we consider is the monotonically increasing Sine-Hyperbolic.

$$\theta_\phi(x) = \alpha \sinh(\beta x)$$

where α and β are the scaling parameters. The β parameter determines the extent of the non-linear re-weighting of the original activation values. As such, it effectively controls the amount of influence higher valued activations have on the average pooling operation performed later on. The α parameter has two important roles: (1) normalising the values of the scaled activations, (2) weighting the multi-layer aggregation streams to compute the optimal global descriptor. The set of parameters associated with this activation function is: $\mathbf{w}_\theta = (\alpha, \beta)$.

Since Sine-Hyperbolic function is differentiable, the chain-rule can be readily applied to obtain the partial derivatives required for back-propagation:

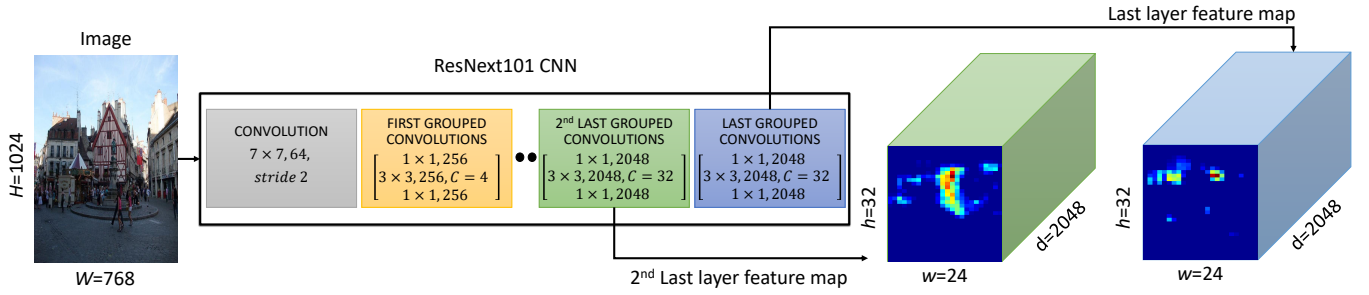
$$\begin{aligned} \frac{\partial \theta_\phi}{\partial x} &= \alpha \beta \cosh(\beta x) \\ \frac{\partial \theta_\phi}{\partial \alpha} &= \sinh(\beta x) \\ \frac{\partial \theta_\phi}{\partial \beta} &= \alpha x \cosh(\beta x) \end{aligned}$$

Exponential function (Exp)

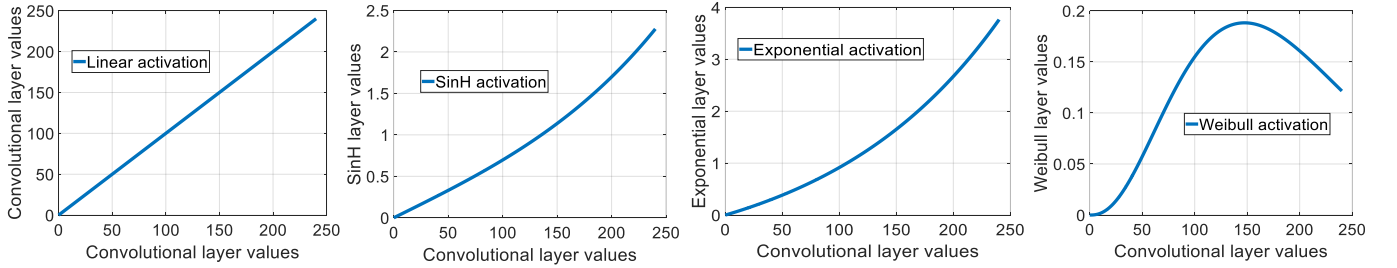
The second activation function that is used to improve the SNR of feature map is based on Exponential function:

$$\theta_\phi(x) = \alpha(\exp(\beta x) - 1)$$

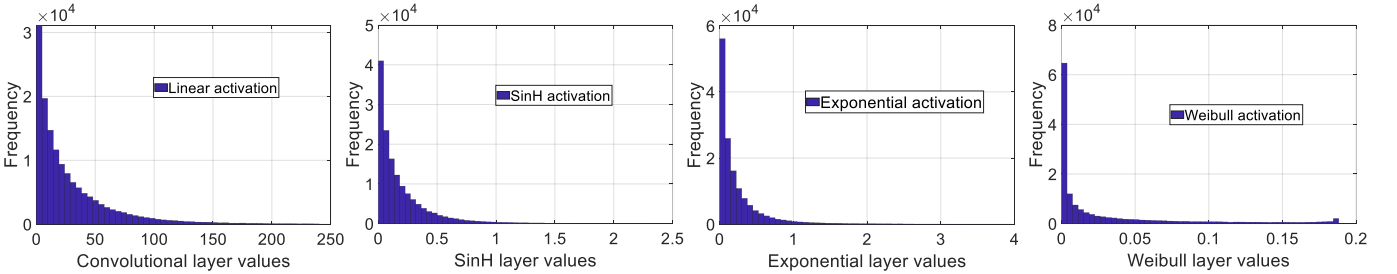
where α and β are the scaling parameters. These play the same role as the α, β parameters in the SinH activation function described above. Thus, the set of parameters associated



(a) An illustration of how the inputs to the activation functions are generated. The output tensor from the final convolutional layer is passed to one of the activation function shown below.



(b) The profile curves of the activation functions considered in this paper: Sine-Hyperbolic, Exponential and Weibull.



(c) The histogram of feature map values before and after passing through activation functions.

Fig. 2. This figure shows the different activation function profiles.

with this function is given as: $\mathbf{w}_\theta = (\alpha, \beta)$. The partial derivatives used for learning for the exponential function are as follows:

$$\begin{aligned} \frac{\partial \theta_\phi}{\partial x} &= \alpha \beta \exp(\beta x) \\ \frac{\partial \theta_\phi}{\partial \alpha} &= \exp(\beta x) - 1 \\ \frac{\partial \theta_\phi}{\partial \beta} &= \alpha x \exp(\beta x) \end{aligned}$$

Modified Weibull function (WB)

Finally, we propose to transform the input values by applying modified Weibull function:

$$\theta_\phi(x) = \begin{cases} \left(\frac{x}{\alpha}\right)^{\beta-1} \exp(-(x/\gamma)^\zeta) & , x \geq 0 \\ 0 & , \text{otherwise} \end{cases}$$

with parameters: $\mathbf{w}_\theta = (\beta, \alpha, \gamma, \zeta)$. Here β is known as the shape parameter and determines where the peak of this activation function will be. The Weibull function is a product of two terms, one increasing at polynomial rate $(x/\alpha)^{\beta-1}$, but another term that is decreasing at an exponential rate $\exp(-(x/\gamma)^\zeta)$. For small enough values, the polynomial term dominates, thus the effect of this activation function is

to non-linearly increase these values. However, eventually the inverse exponential term starts to dominate, thereby reducing the overall activation as the input value further increases. The point x_0 where activation values change from being increased to being decreased can be found by solving $\partial \theta_\phi / \partial x = 0$ for x :

$$x_0 = \gamma \left(\frac{\beta - 1}{\zeta} \right)^{1/\zeta}$$

When we consider how the Weibull function changes the result of the average pooling operation later, we find that it does two fundamentally different forms of reweighting: 1) tensor values before x_0 will have a non-linearly greater influence (polynomial rate), the closer they are to x_0 ; 2) tensor values after x_0 are effectively "balanced", where they exert an exponentially decreasing influence as they get larger.

We note that the partial derivatives are all 0 for values of negative x . In the case where $x \geq 0$, the partial derivatives

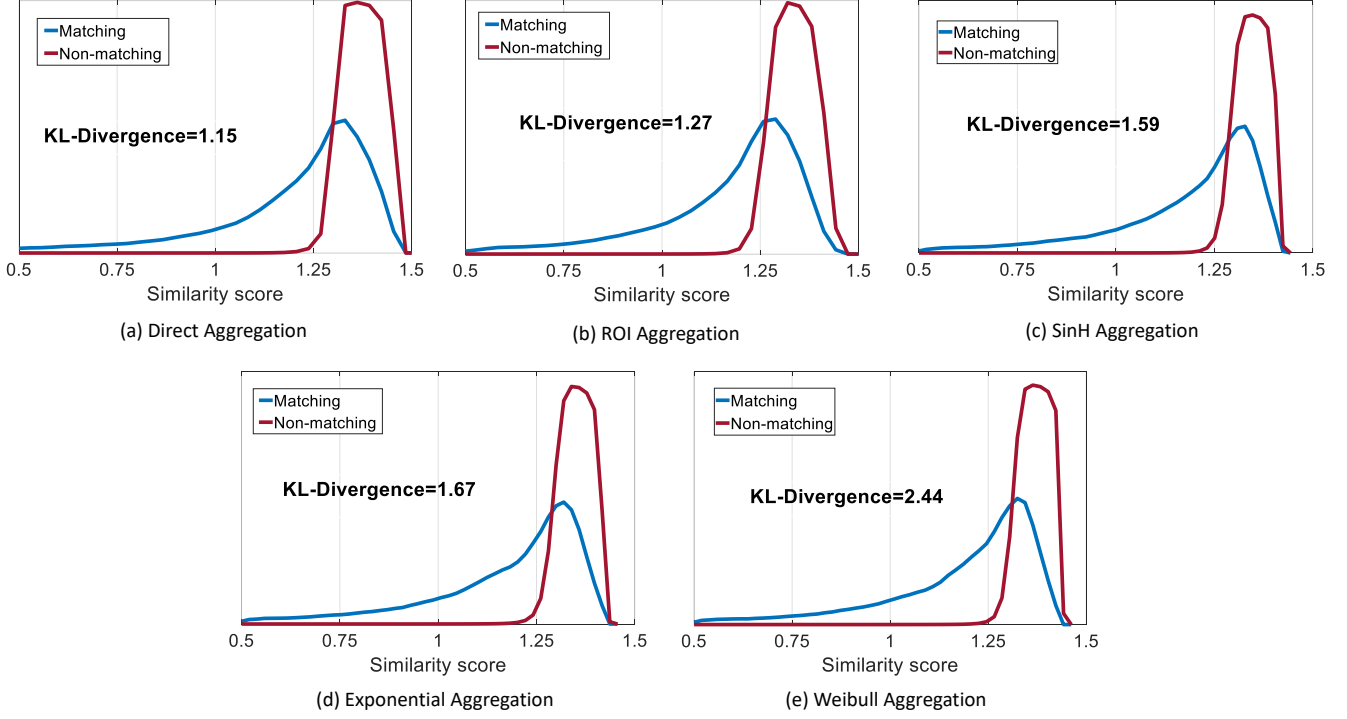


Fig. 3. Histogram of Euclidean distances between matching and non-matching descriptors, for different aggregation methods

are:

$$\begin{aligned} \frac{\partial \theta_\phi}{\partial x} &= \left(\frac{\beta - 1}{\alpha} \right) \left(\frac{x}{\alpha} \right)^{\beta-2} \exp(-(x/\gamma)^\zeta) - \\ &\quad \frac{\zeta}{\gamma^\zeta} \left(\frac{x}{\alpha} \right)^{\beta-1} x^{\zeta-1} \exp(-(x/\gamma)^\zeta) \\ \frac{\partial \theta_\phi}{\partial \beta} &= \log \left(\frac{x}{\alpha} \right) \left(\frac{x}{\alpha} \right)^{\beta-1} \exp(-(x/\gamma)^\zeta) \\ \frac{\partial \theta_\phi}{\partial \alpha} &= (1 - \beta) \left(\frac{x^{\beta-1}}{\alpha^\beta} \right) \exp(-(x/\gamma)^\zeta) \\ \frac{\partial \theta_\phi}{\partial \gamma} &= \zeta \left(\frac{x^{\beta+\zeta-1}}{\alpha^{\beta-1}\gamma^{\zeta+1}} \right) \exp(-(x/\gamma)^\zeta) \\ \frac{\partial \theta_\phi}{\partial \zeta} &= \left(\frac{x}{\alpha} \right)^{\beta-1} \left(-\frac{x}{\gamma} \right)^\zeta \log \left(\frac{x}{\zeta} \right) \exp(-(x/\gamma)^\zeta) \end{aligned}$$

The above three activation functions are integrated into the ACTNET architecture in Section 3.3. However, we will first analyse how different activation functions effect the image features in the next section.

3.2 Analysis of activation functions

Figure 2 demonstrates the process of applying activation function to the features. Firstly, an input tensor for the activation function is obtained by extracting selected convolutional layer output from base CNN (here ResNext101). The elements of this tensor falls inside some non-negative range (Figure 2a). We now apply different functions for non-linearly scaling the values of tensor elements. The transformation of input tensor values by the activation functions considered are shown in Figure 2b. Here, it can be seen that the three activation functions have different degrees of non-linear increase. Importantly, the addition of activation layer

before aggregation gives us a significant improvement over direct aggregation (Section 4). The SinH function provides a non-linear increase that is in between the linear curve and exponential curve. The Exponential function scales up the input values more steeply than SinH. Finally, we see that the Weibull function provides us with a non-linear increase up to a certain point, before its activation values starts decreasing: input values that are overly high (due to noise) are not given a disproportionately high scale. This is crucial as few high activations corresponding to the background in an image could negatively impact the aggregation process.

The distribution of tensor element values before and after passing through the activation functions is presented in Figure 2c. The activation functions significantly improves the SNR of feature map by squeezing majority of noisy responses to significantly small values. Importantly, the Weibull function results in a distribution with a large peak at first bin and also a small peak at last bin of distribution.

The application of activation functions to the feature map values modifies the underlying distributions of the similarity scores for matching and non-matching pairs of images. To demonstrate the importance of activation layer, we compute the class-separability between matching and non-matching descriptors. The descriptors are extracted using the following aggregation approaches:

- 1) Direct aggregation (DA) [18]: the features from the last convolution layers are aggregated using average pooling
- 2) Region of Interest based aggregation (ROIA) [1]: the features are first max-pooled across several multi-scale overlapping regions. The regional descriptors are aggregated using sum pooling

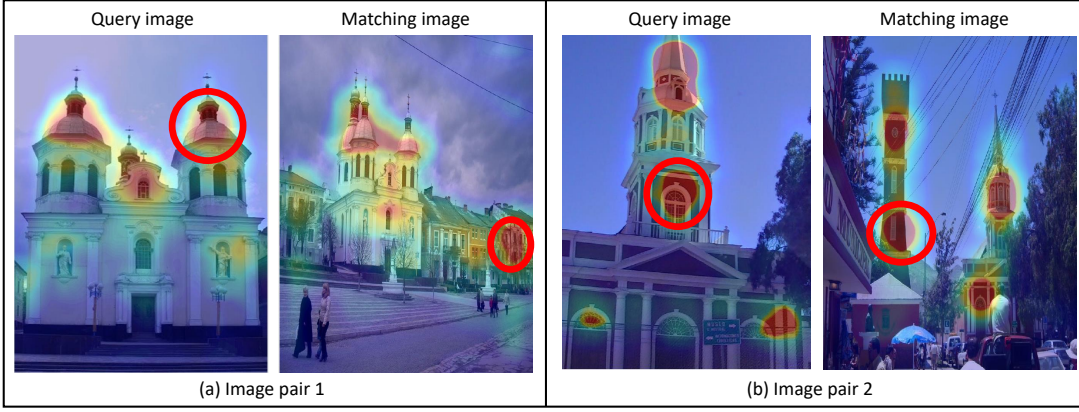


Fig. 4. Visualisation of feature maps of the last convolutional layer for two pair of images: each comprising of a query image and a matching image.

- 3) SinH aggregation (SinHA): the last layers features are transformed using Sine-Hyperbolic function before aggregation using average pooling
- 4) Exponential aggregation (ExpA): the features are passed through Exponential activation layer before pooling.
- 5) Weibull aggregation (WBA): the features are transformed using Weibull activation layer before aggregation.

In all the aforementioned methods, the aggregated signatures are PCA+Whitened and L2-normalised to form global descriptor. We then compute $P(s/m)$ and $P(s/n)$ as the probability of observing a Euclidean distance s for a matching and a non-matching descriptor pair respectively. The separability between $P(s/m)$ and $P(s/n)$ is computed using KL-Divergence (KLD). It can be observed from Figure 3 that the aggregation methods based on activation functions, SinHA (KLD=1.59), ExpA (KLD=1.67), WBA (KLD=2.44), provide better separability between matching and non-matching distributions, compared to DA (KLD=1.15) and ROIA (KLD=1.27). It can also be observed that Weibull aggregation achieves maximum KL-Divergence of 2.44. Importantly, we find that the amount of increase in the KL-divergence correlates strongly with the increase in retrieval accuracy, as shown in Section 4.

In Figure 4 we visualise why it is important to apply activation function before aggregation. We show the last convolutional layer responses for two pair of images: each comprising of a query image and a matching image. The strongest responses are indicated by red circle. The Max-pooling method of [17] generates global descriptors from query image and matching image that have a very low similarity score (Euclidean distance 1.42): the maximum activation for matching image is from the background and not the actual object to be retrieved. The Average-pooling [18] method alleviates the problem of Max-pooling, however the matching descriptor is now contaminated with significant amount of background responses resulting is low similarity score (Euclidean distance 1.39). The application of SinH and Exponential function to the input tensor significantly improves the signal-to-noise ratio thereby increasing the similarity score between global descriptors (Euclidean distance 1.27 and 1.25). One issue with the monotonically increasing

functions SinH and Exp is that they weight the background activation higher than the activations from the actual object thereby negatively impacting the similarity between query image and matching image. The Weibull function decreases the influence of overly high background activations thus providing the highest similarity score (Euclidean distance 1.08).

3.3 Image retrieval ACTNET architecture

We will now formally describe the ACTNET architecture. First, let $\mathbf{x} \in \mathbb{R}^{W \times H \times 3}$ denote an RGB input image of resolution $W \times H$. Next, for the selected base CNN, given an input image \mathbf{x} , suppose we are interested in using K of its convolutional layer outputs ($K = 2$ in ACTNET). Let us denote these K convolutional layers as functions: $f_1(\mathbf{x}), f_2(\mathbf{x}), \dots, f_K(\mathbf{x})$. Associated with each of these functions are their own set of learnable parameters, which are optimised via back-propagation using the partial derivatives $\partial\theta_\phi/\partial x$ given in Section 3.1. These convolutional outputs are then be passed as inputs to their own ‘‘aggregation streams’’ as described next.

Aggregation stream

The aim of the aggregation stream is to perform non-linear scaling and aggregation of convolutional features. First, the input tensor $\mathbf{X} \in \mathbb{R}^{W \times H \times D}$ is transformed using the activation function ϕ resulting in output tensor $\mathbf{Y} \in \mathbb{R}^{W \times H \times D}$

$$\mathbf{Y} = \phi(\mathbf{X}; \theta_\phi, \mathbf{w}_\theta)$$

We next apply global average pooling denoted by $P(\mathbf{Y})$:

$$P(\mathbf{Y}) = \left(\frac{1}{WH} \sum_i^W \sum_j^H y_{ijk} \right)_{k=1}^D$$

The output of the global average pooling operation is the vector $\mathbf{z} = P(\mathbf{Y})$, which we normalise to balance the severity of increase in values due to the non-linear scaling process of the activation layer. In our work, we have found that the choice of fractional power achieves best results. The normalisation function is denoted as $\psi : \mathbb{R}^D \rightarrow \mathbb{R}^D$, with the rule:

$$\psi(\mathbf{z}) = \lambda z_1^p, \lambda z_2^p, \dots, \lambda z_D^p$$

where λ, p are learnable scaling parameters.

To bring it all together, we can now define the full aggregation stream as the function: $\Phi : \mathbb{R}^{W \times H \times D} \rightarrow \mathbb{R}^D$, with the rule:

$$\Phi(\mathbf{X}) = \psi(P(\phi(\mathbf{X}; \theta_\phi, \mathbf{w}_\theta))) \quad (1)$$

To aid the following discussion when multiple streams are considered, we gather all the learnable parameters described above into a set denoted as:

$$\eta = \{\mathbf{w}_\theta, p, \lambda\} \quad (2)$$

Global descriptor generation

We now describe how the global descriptor of an image \mathbf{x} will be generated using convolutional features from the base-CNN.

As noted previously, we are interested in using K convolutional layer outputs from the base-CNN. Each such convolutional layer gives rise to a separate aggregation stream of form Eq. 1. We denote each of the K separate streams as: $\Phi_1(f_1(\mathbf{x})), \Phi_2(f_2(\mathbf{x})), \dots, \Phi_K(f_K(\mathbf{x}))$. Their respective learnable parameters (Eq. 2) are denoted as: $\eta_1, \eta_2, \dots, \eta_K$. The global descriptor is then constructed by concatenation of the outputs of all aggregation streams:

$$\mathbf{b} = [\Phi_1(f_1(\mathbf{x})), \Phi_2(f_2(\mathbf{x})), \dots, \Phi_K(f_K(\mathbf{x}))]$$

The concatenated feature vector \mathbf{b} is then passed to a PCA and whitening layer, before given to an L2-normalisation layer, which produces the final global descriptor used for image retrieval.

3.4 End-to-end training of ACTNET

A vital aspect of the ACTNET is that all its components are considered to represent differentiable operations. Our novel activation layer is differentiable with parameters that can be optimised during training. The average pooling layer and the normalisation layer are also differentiable. The PCA+Whitening projection can be implemented as a Fully Connected layer (for the projection with the whitened eigenvectors) with bias (for mean subtraction), with weights that can be optimised. In conclusion, the ACTNET is an end-to-end architecture which can learn the convolutional filter weights, activation parameters and PCA+Whitening parameters, using Stochastic Gradient Descent (SGD) on triplet loss function during training.

We will now show how to build ACTNET using the base CNN ResNext101 [4]. The first phase of training starts by fine-tuning ResNext101 (trained on ImageNet) on GLRD dataset using classification loss. In the second phase, we remove the last three layers of the tuned ResNext101 and add the activation layers, average pooling layers and normalisation layers to the last two convolutional layers. The outputs from the normalisation blocks are concatenated and a PCA+Whitening layer is added to form the final ACTNET. We then adopt a three stream siamese architecture to train the warmed-up ACTNET using triplet loss. For siamese network training, a dataset of R triplets, each composing of a query image, a matching image and a non-matching image is considered. More precisely let a^q be an ACTNET representation of a query image, a^m be a representation

of a matching image and a^n be a representation of a non-matching image. The triplet loss can be defined as:

$$L = \frac{1}{2} \max(0, t + \|a^q - a^m\|^2 - \|a^q - a^n\|^2), \quad (3)$$

where t controls the margin. During training the aim of the triplet loss is to tune the ACTNET parameters such that the distance between a^q and a^m reduces and distance between a^q and a^n increases.

Given an query image at test time, the ACTNET produces robust and discriminative 4096-dimensional image representation well-suited for image retrieval.

3.5 Low complexity ACTNET

The ACTNET systems based on state-of-the-art CNNs such as VGG, ResNet101, ResNext101 and DenseNet require significant amount of computational resources beyond the capabilities of mobile devices. In this section, we develop a low complexity ACTNET to effectively maximise retrieval performance while being mindful of the limited resources. The overall architecture consists of a baseline CNN MobileNetV2 followed by our aggregation system. The pipeline to create low complexity ACTNET (Mobile-ACTNET) is as follows: we remove the last pooling layer, prediction layer and loss layer of MobileNetV2 (trained on ImageNet). The outputs of the final two convolutional layers are then passed to activation layers, average pooling layers, normalisation layers and concatenation layer, generating a global descriptor. Finally, a three stream siamese network is adopted to train Mobile-ACTNET on GLDR dataset using triplet loss.

Given a query image at test time, the ACTNET generates a 2560 dimensional image signature. The dimensionality of the final signature is reduced to 1280-dimensional using PCA+Whitening transformation, thereby reducing the memory requirements and increasing the matching speed.

In all the following experiments, we will call ResNext based ACTNET as "ACTNET" and MobileNetV2 based ACTNET as "Mobile-ACTNET".

4 EXPERIMENTAL RESULTS

In this section we detail the implementation details of our architecture and give qualitative and quantitative results to validate our method. We first describe the experimental setup which includes the training parameters, training and test datasets and evaluation protocols. We then discuss the importance of the novel components of ACTNET, namely the robust activation function and Multi-layer aggregation. Finally, we compare the proposed method to the state-of-the-art, showing significant improvement in retrieval performance.

4.1 Training setup

We train ACTNET on a subset of Google Landmarks dataset (GLD) [37], which contains 1 Million images depicting 15K unique landmarks (classes). In GLD the number of images per class are highly unbalanced, some classes are associated to thousands of images, while for around 10K classes only 10 or fewer images are present. Furthermore, the GLD contains a non-negligible fraction of images unrelated to the

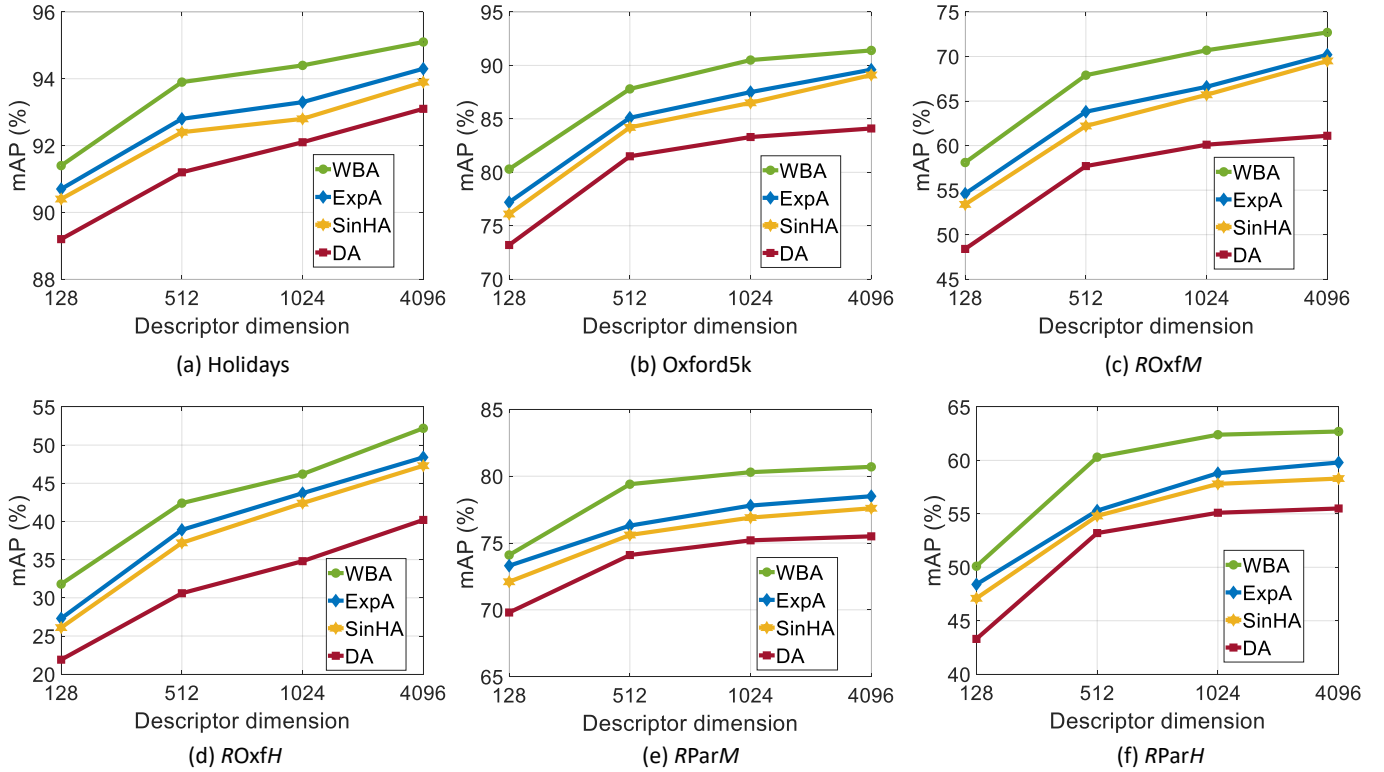


Fig. 5. Comparison of retrieval performance with different aggregation methods: Direct aggregation (DA), SinH aggregation (SinHA), Exponential aggregation (ExpA) and Weibull aggregation (WBA) on (a) Holidays, (b) Oxford5k, (c) *ROxfM*, (d) *ROxfH*, (e) *RParM*, (f) *RParH*, (all results in mAP(%));

landmarks. For this reason, we pre-process the GLD using RVDW global descriptor and SIFT based RANSAC [31], to obtain a clean dataset containing 200K images belonging to 2K classes. Finally, to guarantee unbiased evaluation we remove all images that overlap Oxford, Paris, Holidays and MPEG datasets. We refer this clean dataset as Google Landmarks Retrieval dataset (GLRD).

We adopt a siamese architecture and train the ACTNET on GLDR dataset using triplet loss. The objective function is optimised by Stochastic Gradient Descent (SGD), with learning rate 1e-03, weight decay of 5e-04, momentum 0.9 and triplet loss margin 0.1. Each triplet contains 1 query, 1 matching and 1 non-matching image and the size of each image is fixed to 1024×768. To ensure that the sampled triplets incur loss and help in the training process, we extract the global descriptors from GLRD using the current model, and compute 5k triplets : each triplet contains a query, a matching and hardest non-matching images. All the triplets that incur a loss are sent to the network for training. After each epoch (training on 5K triplets), our algorithm generates a new set of 5K triplets using the current model. The training process is performed for at most 20 epochs. We overcome the *TITANX* GPU memory limitation of 11GB by processing one triplet at a time and updating the gradients after every 64 triplets.

4.2 Test datasets and evaluation protocol

The original Oxford5k dataset contains 5063 high-resolution images, with a subset of 55 images used as queries. In [38],

Radenovic et al. revisited the original Oxford dataset to correct annotation errors, add 15 new challenging queries and introduce new evaluation protocols. The revisited Oxford dataset (*ROxf*) comprise of 4993 images with 70 queries used for evaluation.

The revisited Paris dataset (*RPar*) is a modified version of Paris6K dataset: there are 70 query images with 6322 database images.

The Holidays datasets [39] consists of 1491 Holidays pictures, 500 of them are as queries. Following the standard procedure, we manually correct the orientation of the images.

The Motion Picture Experts Group (MPEG) dataset is a collection of 35K images from five image categories: (1) Graphics, (2) Paintings, (3) Video frames, (4) Landmarks and (5) Common objects. A total of 8313 queries are used to measure the retrieval performance.

To evaluate system performance in a more challenging scenario, the Holidays, Oxford5k, *ROxf* and *RPar* datasets are augmented with a distractor set containing 1Million images (*R1M*). The retrieval performance for all datasets is computed using mean Average Precision(mAP). We follow the standard protocol for *ROxf* and *RPar* datasets and report results using medium and hard setups referred as *ROxfM*, *RParM*, *ROxfH* and *RParH*.

4.3 Impact of activation layer

This experiment investigates the importance of applying activation functions to deep features. The baseline is Direct

TABLE 1
Importance of Multi-layer aggregation of convolutional features

	Holidays	Oxford5k	ROxfM	ROxfH	RParM	RParH	MPEG
SLA	94.1	88.9	68.9	45.5	78.9	59.8	78.9
MLA	95.1	91.4	72.7	52.2	80.7	62.7	82

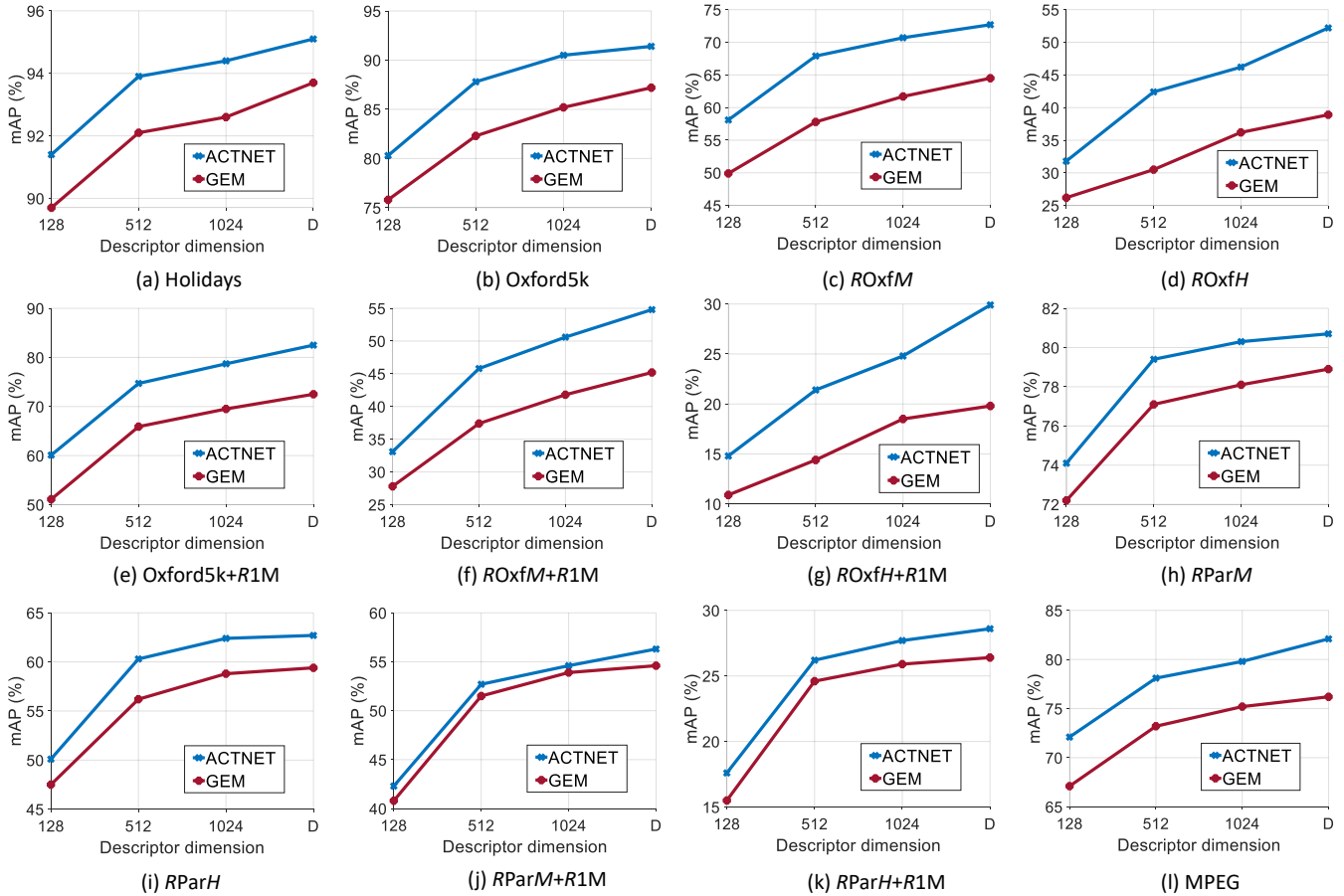


Fig. 6. ACTNET comparison with state-of-the-art GEM network (a) Holidays, (b) Oxford5k, (c) *ROxfM*, (d) *ROxfH*, (e) Oxford5k+R1M, (f) *ROxfM+R1M*, (g) *ROxfH+R1M*, (h) *RParM*, (i) *RParH*, (j) *RParM+R1M*, (k) *RParH+R1M*, (l) MPEG, (all results in mAP(%));

aggregation (DA) method where the convolutional layer features are simply aggregated using average pooling. We compare the baseline performance with the proposed SinH aggregation (SinHA), Exponential aggregation (ExpA) and Weibull aggregation (WBA) methods. It can be observed from Figure 5 that it is essential to apply activation functions to the features before aggregation to obtain significant increase in the retrieval accuracy. The Weibull aggregation provides average gains of 10.5%, 11.3%, 4.9% and 7.1% on *ROxfM*, *ROxfH*, *RParM* and *RParH*, over Direct aggregation. Furthermore, the WBA network also outperforms ExpA and SinHA on all datasets.

In all the following experiments and comparison with the state-of-the-art, we will use Weibull aggregation in ACTNET.

4.4 Impact of multi-layer aggregation

This section demonstrates the advantage of aggregating a hierarchy of convolutional features from multiple CNN

layers. In ACTNET, deep features from the last two convolutional layers of ResNext101 are transformed using activation layers, aggregated via average pooling and concatenated to form image representation. Importantly, the trainable parameters of the two aggregation streams are optimised explicitly to achieve significant retrieval improvement. It can be observed from Table 1 that multi-layer aggregation (MLA) brings an improvement of +1.0%, +2.5% and 3.1% on Holidays, Oxford5k and MPEG datasets compared to single layer aggregation (SLA), where only the last layer features are used to compute global descriptor. The gain in retrieval accuracy is even more pronounced on difficult datasets: 6.7% and 2.9% on *ROxfH* and *RParH* datasets.

4.5 Comparison of GEM and ACTNET

In this section we compare ACTNET with the state-of-the-art GEM network. To get a fair assessment, we train both ACTNET and GEM in an end-to-end manner on GLDR dataset with triplet loss. In GEM, the generalised mean pooling layer [2] is added to the last convolutional layer

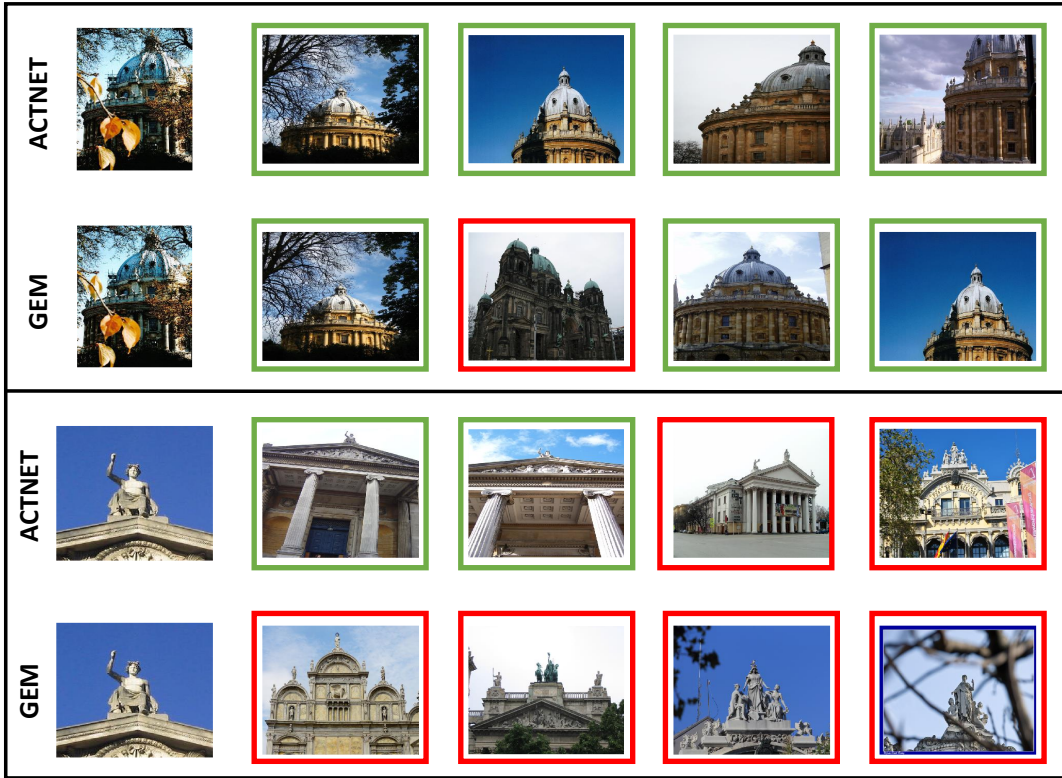


Fig. 7. Top four retrieved images for ACTNET and GEM on *ROxford* datasets. On the plot, the correctly retrieved images for a particular query are marked with green border and falsely retrieved images are marked with red border

of the ResNext101. The pooling layer is followed by L2-normalisation, PCA+Whitening and L2-normalisation layers.

After training the networks, we extract ACTNET and GEM representations from the test datasets and compute the retrieval performance (Figure 6), as a function of descriptor dimensionality D . Compared to GEM, ACTNET offers a gain of +1.7%, 4.8% and 5.1% on Holidays, Oxford5k and MPEG datasets. The average difference in retrieval accuracy is even more significant on challenging datasets of *ROxfM* (+8.8%), *ROxfH* (+10.2%) and *RParH* (+3.4%). On large scale datasets of *ROxfM+R1M*, *ROxfH+R1M*, *RParM+R1M* and *RParH+R1M* dataset, ACTNET achieves 54.8%, 29.9%, 56.3% and 28.6%, outperforming any results published to date. It is also important to note to ACTNET short signature (128D) consistently achieves higher mAP than GEM 128D signature on all datasets.

Figure 7 illustrates top four retrieved images by our ACTNET and baseline GEM on few *ROxf* queries. For every query, the correctly retrieved images are marked by green frame. It can be observed that in both the cases ACTNET is able to retrieve difficult matching images compared to GEM, that places them far down in the rank.

4.6 Performance of low complexity ACTNET

In this section, the retrieval performance of low complexity Mobile-ACTNET is evaluated. The Mobile-ACTNET is a low depth, low latency and small memory model, developed to effectively maximise retrieval accuracy while being mindful of the limited resources of mobile device. It can be

seen from Figure 8 that the performance of Mobile-ACTNET is on average 8% less than ACTNET. However, the descriptor extraction speed of Mobile-ACTNET is approximately five times faster than ACTNET.

We also compare the performance of Mobile-ACTNET with the computationally complex state-of-the-art ResNet101-GEM [2] and ResNet101-RMAC [1]. We compute single-scale representations of ResNet101-GEM and ResNet101-RMAC using the software provided by the authors. It is interesting to observe from Table 2 that Mobile-ACTNET achieves comparable performance that the aforementioned methods while having five times faster extraction speed.

TABLE 2
Mobile-ACTNET comparison with state-of-the-art ResNet101-GEM and ResNet101-RMAC representations

	Hol	Oxf5k	<i>ROxfM</i>	<i>ROxfH</i>	MPEG
Mobile-ACTNET	92.9	85.1	61.1	35.5	73.1
ResNet101-GEM	92.4	85.7	61.7	35.1	74.1
ResNet101-RMAC	94.0	84.1	60.9	32.4	72.2

5 COMPARISON WITH THE STATE-OF-THE-ART

We extensively compare the performance of ACTNET with the state-of-the-art on compact image signatures and on methods that use query expansion.

The performance of the full dimensional image signatures (1K-4K Dimensions) is summarised in Table 3. In real

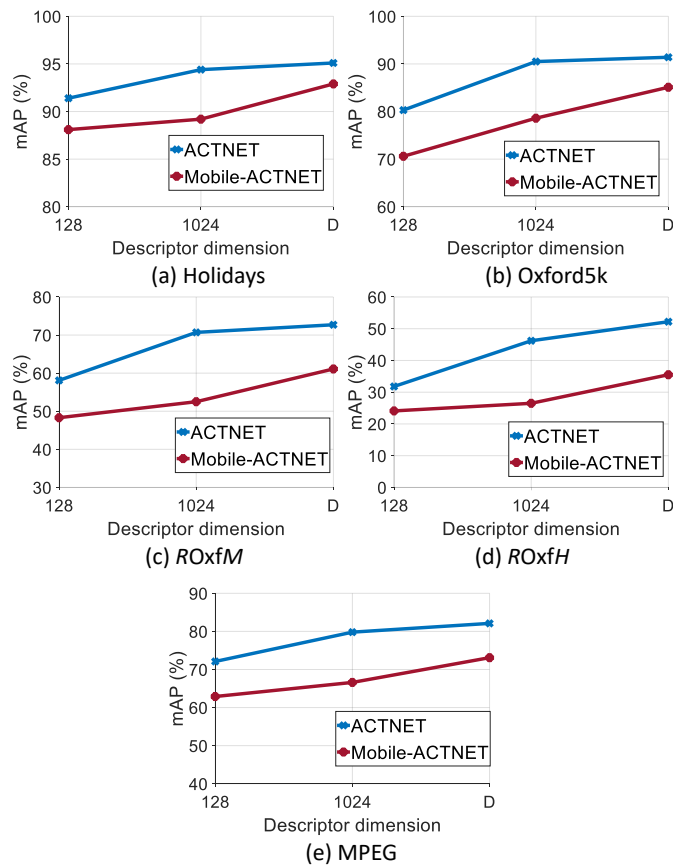


Fig. 8. Low complexity Mobile-ACTNET comparison with ACTNET (a) Holidays, (b) Oxford5k, (c) *ROxM*, (d) *ROxH*, (e) MPEG (all results in mAP(%));

world scenarios containing billions of images, the use of image representations with dimensionality greater than 1K is prohibitive due to memory requirements and search time. However, we will use these results to find the maximum performance of global image representations.

The proposed ACTNET consistently outperforms the state-of-the-art on all datasets. Compared to RMAC [1], ACTNET provides a significant gain of +5.3%, +11.8%, 1.8% and 9.9% in mAP on Oxford5k, *ROxM*, *RParM* and MPEG datasets. The difference in mAP points between ACTNET and RMAC is even higher on challenging datasets (+19.8% *ROxH*, +15.5% *ROxM+R1M*, +17.4% *ROxM+R1M*, +3.3% *RParH* and +1.5% *RParM+R1M*). Compared to the best competitor GEM representation [2], ACTNET is more than 13.7, 9.6, 10, 6.4 and 3.9 mAP points ahead on *ROxH*, *ROxM+R1M*, *ROxH+R1M*, *RParH* and *RParH+R1M* datasets. It is important to note that our ACTNET representation is computed from single scale compared to RMAC [1] and GEM [2] representations where 3 image scales are used. We also compare ACTNET with our implementation of ResNext+GEM and the retrieval accuracy show that ACTNET is significantly more robust and discriminative image signature.

It has recently become a common practice to apply Query Expansion (QE) on top of global image signatures to further improve the retrieval accuracy. More precisely, we use α query expansion [2] and diffusion (DFS) [40]. It

can be observed from Table 4 that ACTNET+ α QE achieves significantly better mAP compared to RMAC+ α QE and GEM+ α QE. Furthermore, ACTNET+DFS achieves 70.7%, 49.1%, 88.9% and 78.4% on *ROxM+R1M*, *ROxH+R1M*, *RParM+R1M* and *RParH+R1M* datasets, outperforming the best published results. It is also interesting to note that ACTNET+DFS outperforms computationally complex DELF-D2R-R-ASMK+SP approach which uses CNN based local features, codebook of 65k visual words and Spatial Verification (SP).

Finally, we compare the retrieval performance of compact (128-D) image signatures which are practicable in real world applications. To compute a compact signature, we forward pass an image through ACTNET to obtain 4094-D representation. Top 128 dimensions of 4096-D descriptors forms the compact signature. The results presented in Table 5 show that ACTNET significantly outperforms state-of-the-art RMAC and GEM methods. On large scale datasets of *ROxM+R1M*, *ROxH+R1M*, *RParM+R1M* and *RParH+R1M*, ACTNET achieves the best ever performances of 33.1%, 14.8%, 42.3% and 17.6% respectively.

6 CONCLUSION

In this paper we introduced a novel CNN network architecture called ACTNET. The key innovation is a novel trainable activation layer designed to improve the signal-to-noise ratio in the aggregation stage of deep convolutional features. Our activation layer amplifies a few selected strong filter responses (corresponding to prominent features) thus reducing the impact of weaker features, which effectively constitute background noise. In ACTNET, deep features from final convolutional layers are transformed using activation function and optimally aggregated into a global descriptor.

The parameters of activation blocks are trained jointly with the CNN filter parameters in an end-to-end manner by minimising the triplet loss. We proposed and evaluated three parametric activation functions: Sine-Hyperbolic, Exponential and modified Weibull, showing that while all bring significant gains, the Weibull achieved the best performance thanks to its equalising properties. As far as we are aware this is the first time activation layer is designed and trained to learn optimal aggregation.

We provided a thorough evaluation on all key benchmarks demonstrating that ACTNET architecture with learnable aggregation generates global representations that significantly outperform the latest state-of-the-art methods, including those based on computationally costly local descriptor indexing and spatial verification. We also show that ACTNET retains its leading performance when using short codes of 128 bytes and when applied to low-complexity CNN.

REFERENCES

- [1] J. R. J. Gordo, Albertand Almazán and D. Larlus, "End-to-end learning of deep visual representations for image retrieval," *International Journal of Computer Vision*, vol. 124, no. 2, Sep 2017.
- [2] F. Radenovi, G. Tolias, and O. Chum, "Fine-tuning CNN image retrieval with no human annotation," *IEEE Transactions on Pattern Analysis and Machine Intelligence*, pp. 1–1, 2018.

TABLE 3

Comparison with the state-of-the-art using full dimensional descriptor on Oxford5k, *ROxford* Medium protocol (*ROxfM*), *ROxford* Hard protocol (*ROxfH*), *RParis* Medium protocol (*RParM*), *RParis* Hard protocol (*RParH*), Holidays and MPEG without and with one Million distractors (*R1M*). All results are computed in terms of mAP(%). The results for MPEG datasets are computed using the software provided by the authors

	Oxford 5k	<i>ROxfM</i>	<i>ROxfH</i>	<i>ROxfM+R1M</i>	<i>ROxfH+R1M</i>	<i>RParM</i>	<i>RParH</i>	<i>RParM+R1M</i>	<i>RParH+R1M</i>	Hol	MPEG
NetVLAD [22]	71.6	37.1	13.8	20.7	6.0	59.8	35	31.8	11.5	87.5	65.1
SPoC [41]	68.1	39.8	12.4	21.5	2.8	69.2	44.7	41.6	15.3	83.9	63.2
CroW [20]	70.8	42.4	13.3	21.2	3.3	70.4	47.2	42.7	16.3	85.1	68.2
MAC [38]	80	41.7	18	24.2	5.7	66.2	44.1	40.8	18.2	85.5	70.6
AGEM [28]	-	67	40.7	-	-	78.1	57.3	-	-	-	-
FS.EGM [42]	-	63	34.5	-	-	68.7	43.9	-	-	-	-
OS.EGM [42]	-	64.2	35.9	-	-	69.9	46.1	-	-	-	-
ASDA [29]	87.7	66.4	38.5	-	-	71.6	47.9	-	-	-	-
GEM [38]	87.8	64.7	38.5	45.2	19.9	77.2	56.3	52.3	24.7	93.9	74.1
RMAC [38]	86.1	60.9	32.4	39.3	12.5	78.9	59.4	54.8	28.0	94.8	72.2
ResNext+GEM	87.2	64.5	38.9	45.2	19.8	78.8	59.5	54.6	26.4	93.7	76.2
ACTNET	91.4	72.7	52.2	54.8	29.9	80.7	62.7	56.3	28.7	95.1	82.1

TABLE 4

Performance evaluation of full dimensional image signatures using Query Expansion

	<i>ROxfM</i>	<i>ROxfH</i>	<i>ROxfM+R1M</i>	<i>ROxfH+R1M</i>	<i>RParM</i>	<i>RParH</i>	<i>RParM+R1M</i>	<i>RParH+R1M</i>
DELFD2R-R-ASMK+SP [30]	71.9	48.5	-	-	78	54	-	-
DELFDGLD-ASMK+SP [30]	76	52.4	-	-	80.2	58.6	-	-
GEM+ α QE [38]	67.2	40.8	49	24.2	80.7	61.8	58	31
RMAC+ α QE [38]	64.8	36.8	45.7	19.5	82.7	65.7	61	35
ResNext-GEM+ α QE	70.4	43.5	51.5	25.3	82.6	65.5	62.1	35.5
ACTNET+ α QE	77.2	56.6	61.5	36.3	84.6	68.6	65.6	40.9
GEM+DFS [38]	69.8	40.5	61.5	33.1	88.9	78.5	84.9	71.6
RMAC+DFS [38]	69.0	44.7	56.6	28.4	89.5	80.0	83.2	70.4
ACTNET+DFS	78.3	57.1	70.7	49.1	91.1	83.1	88.9	78.4

TABLE 5

Comparison with the state-of-the-art using small dimensional descriptor (128-Dim). The results for RMAC and GEM are computed using the software provided by authors

	Dim	Holidays	Oxford5k	<i>ROxfM</i>	<i>ROxfH</i>	<i>ROxfM+R1M</i>	<i>ROxfH+R1M</i>	<i>RParM</i>	<i>RParH</i>	<i>RParM+R1M</i>	<i>RParH+R1M</i>
RMAC [1]	128	88.5	77.9	46.2	21.1	21.9	7.4	73.2	48.9	41.5	16.5
GEM [2]	128	85.9	79.5	49.9	26.2	27.8	10.9	72.2	47.5	40.8	15.5
ACTNET	128	91.4	80.3	58.1	31.8	33.1	14.8	74.1	50.1	42.3	17.6

[3] G. Tolias, R. Sivic, and H. Jégou, "Particular object retrieval with integral max-pooling of cnn activations," *CoRR*, 2015.

[4] S. Xie, R. Girshick, P. Dollr, Z. Tu, and K. He, "Aggregated residual transformations for deep neural networks," in *2017 IEEE Conference on Computer Vision and Pattern Recognition (CVPR)*, July 2017.

[5] M. Sandler, A. Howard, M. Zhu, A. Zhmoginov, and L. Chen, "Mobilenetv2: Inverted residuals and linear bottlenecks," in *IEEE Conference on Computer Vision and Pattern Recognition*, June 2018, pp. 4510–4520.

[6] D. G. Lowe, "Distinctive image features from scale-invariant keypoints," *International Journal of Computer Vision*, pp. 91–110, 2004.

[7] H. Bay, A. Ess, T. Tuytelaars, and L. Van Gool, "Speeded-up robust features (SURF)," *Computer Vision and Image Understanding*, pp. 346–359, 2008.

[8] J. Sivic and A. Zisserman, "Video Google: A text retrieval approach to object matching in videos," in *IEEE International Conference on Computer Vision*, vol. 2, 2003, pp. 1470–1477.

[9] F. Perronnin, Y. Liu, J. Sanchez, and H. Poirier, "Large-scale image retrieval with compressed fisher vectors." in *IEEE Conference on Computer Vision and Pattern Recognition*, 2010, pp. 3384–3391.

[10] H. Jégou, F. Perronnin, M. Douze, J. Sánchez, P. Pérez, and C. Schmid, "Aggregating local image descriptors into compact codes," *IEEE Transactions on Pattern Analysis and Machine Intelligence*, pp. 1704–1716, Sep 2012.

[11] H. Jégou and A. Zisserman, "Triangulation embedding and democratic aggregation for image search," in *IEEE Conference on Computer Vision and Pattern Recognition*, 2014.

[12] S. S. Husain and M. Bober, "Improving large-scale image retrieval through robust aggregation of local descriptors," *IEEE Transactions on Pattern Analysis and Machine Intelligence*, vol. 39, no. 9, pp. 1783–1796, Sept 2017.

[13] J. Philbin, O. Chum, M. Isard, J. Sivic, and A. Zisserman, "Object retrieval with large vocabularies and fast spatial matching," in *IEEE Conference on Computer Vision and Pattern Recognition*, 2007.

[14] J. Philbin, M. Isard, J. Sivic, and A. Zisserman, "Lost in quantization: Improving particular object retrieval in large scale image databases," in *IEEE Conference on Computer Vision and Pattern Recognition*, 2008.

[15] O. Chum, A. Mikulík, M. Perdoch, and J. Matas, "Total recall ii: Query expansion revisited," in *CVPR 2011*, June 2011, pp. 889–896.

[16] G. Tolias and H. Jégou, "Visual query expansion with or without geometry: Refining local descriptors by feature aggregation," *Pattern Recognition*, vol. 47, pp. 3466–3476, 2014.

[17] H. Azizpour, A. S. Razavian, J. Sullivan, A. Maki, and S. Carlsson, "Factors of transferability for a generic convnet representation," *IEEE Transactions on Pattern Analysis and Machine Intelligence*, vol. 38, no. 9, pp. 1790–1802, Sept 2016.

[18] A. Babenko, A. Slesarev, A. Chigorin, and V. S. Lempitsky, "Neural codes for image retrieval," in *Computer Vision - ECCV 2014* -

- 13th European Conference, Zurich, Switzerland, September 6-12, 2014, Proceedings, Part I*, 2014, pp. 584–599.
- [19] K. Simonyan and A. Zisserman, “Very deep convolutional networks for large-scale image recognition,” *CoRR*, 2014.
- [20] Y. Kalantidis, C. Mellina, and S. Osindero, “Cross-dimensional weighting for aggregated deep convolutional features,” in *ECCV Workshops*, 2016.
- [21] E. Ong, S. Husain, and M. Bober, “Siamese network of deep fisher-vector descriptors for image retrieval,” *CoRR*, vol. abs/1702.00338, 2017. [Online]. Available: <http://arxiv.org/abs/1702.00338>
- [22] R. Arandjelovic, P. Gronat, A. Torii, T. Pajdla, and J. Sivic, “NetVLAD: CNN architecture for weakly supervised place recognition,” *IEEE Transactions on Pattern Analysis and Machine Intelligence*, vol. 40, no. 6, pp. 1437–1451, June 2018.
- [23] O. Seddati, S. Dupont, S. Mahmoudi, and M. Parian, “Towards good practices for image retrieval based on cnn features,” in *The IEEE International Conference on Computer Vision (ICCV)*, Oct 2017.
- [24] A. Jimenez, J. M. Alvarez, and X. Giro-i Nieto, “Class-weighted convolutional features for visual instance search,” in *28th British Machine Vision Conference (BMVC)*, September 2017.
- [25] J. Xu, C. Wang, C. Qi, C. Shi, and B. Xiao, “Unsupervised semantic-based aggregation of deep convolutional features,” *IEEE Transactions on Image Processing*, vol. 28, no. 2, pp. 601–611, 2019.
- [26] S. Pang, J. Xue, J. Zhu, L. Zhu, and Q. Tian, “Unifying sum and weighted aggregations for efficient yet effective image representation computation,” *IEEE Transactions on Image Processing*, vol. 28, no. 2, pp. 841–852, 2019.
- [27] X. Wu, G. Irie, K. Hiramatsu, and K. Kashino, “Weighted generalized mean pooling for deep image retrieval,” in *2018 25th IEEE International Conference on Image Processing (ICIP)*, 2018, pp. 495–499.
- [28] Y. Gu, C. Li, and J. Xie, “Attention-aware generalized mean pooling for image retrieval,” *CoRR*, 2018.
- [29] J. Xu, C. Wang, C. Shi, and B. Xiao, “Weakly supervised soft-detection-based aggregation method for image retrieval,” *CoRR*, 2018.
- [30] M. Teichmann, A. Araujo, M. Zhu, and J. Sim, “Detect-to-retrieve: Efficient regional aggregation for image search,” *CoRR*, 2018.
- [31] S. S. Husain and M. Bober, “Remap: Multi-layer entropy-guided pooling of dense cnn features for image retrieval,” *IEEE Transactions on Image Processing*, pp. 1–1, 2019.
- [32] K. Jarrett, K. Kavukcuoglu, M. Ranzato, and Y. LeCun, “What is the best multi-stage architecture for object recognition?” in *2009 IEEE 12th International Conference on Computer Vision*, Sep. 2009, pp. 2146–2153.
- [33] X. Glorot and Y. Bengio, “Understanding the difficulty of training deep feedforward neural networks,” in *Proceedings of the Thirteenth International Conference on Artificial Intelligence and Statistics*, vol. 9, 13–15 May 2010, pp. 249–256.
- [34] I. Goodfellow, D. Warde-Farley, M. Mirza, A. Courville, and Y. Bengio, “Maxout networks,” in *Proceedings of the 30th International Conference on Machine Learning*, S. Dasgupta and D. McAllester, Eds., vol. 28, no. 3, 2013, pp. 1319–1327.
- [35] S. Qian, H. Liu, C. Liu, S. Wu, and H. S. Wong, “Adaptive activation functions in convolutional neural networks,” *Neurocomputing*, vol. 272, pp. 204 – 212, 2018.
- [36] F. Agostinelli, M. D. Hoffman, P. J. Sadowski, and P. Baldi, “Learning activation functions to improve deep neural networks,” *CoRR*, vol. abs/1412.6830, 2014.
- [37] H. Noh, A. R. T. S. Araujo, J. Sim, T. Weyand, and B. Han, “Large-scale image retrieval with attentive deep local features,” *2017 IEEE International Conference on Computer Vision (ICCV)*, pp. 3476–3485, 2017.
- [38] F. Radenovic, A. Iscen, G. Tolias, Y. Avrithis, and O. Chum, “Revisiting oxford and paris: Large-scale image retrieval benchmarking,” in *2018 IEEE Conference on Computer Vision and Pattern Recognition*, June 2018, pp. 5706–5715.
- [39] H. Jégou, M. Douze, and C. Schmid, “Improving bag-of-features for large scale image search,” *International Journal of Computer Vision*, feb 2010.
- [40] A. Iscen, G. Tolias, Y. Avrithis, T. Furon, and O. Chum, “Efficient diffusion on region manifolds: Recovering small objects with compact cnn representations,” in *CVPR*, 2017.
- [41] A. B. Yandex and V. Lempitsky, “Aggregating local deep features for image retrieval,” in *2015 IEEE International Conference on Computer Vision (ICCV)*, Dec 2015, pp. 1269–1277.
- [42] O. Siméoni, A. Iscen, G. Tolias, Y. Avrithis, and O. Chum, “Graph-based particular object discovery,” *Machine Vision and Applications*, vol. 30, pp. 243–254, Mar 2019.